Appl Phys B (2011) 105:557–563
DOI 10.1007/s00340-011-4503-6

Applied Physics B
Lasers and Optics

Recent advances in optodynamics

J. Možina · J. Diaci

Received: 23 October 2010 / Revised version: 27 January 2011 / Published online: 9 April 2011

Abstract The term optodynamics has been introduced to describe a wide range of optically induced dynamic phenomena, which play an important role in laser–material processes as well as in laser-assisted medical applications. In view of laser material processing, a laser beam is not only considered as a tool, but also as a generator of information about the material's transformation. The information is retained and conveyed by different kinds of optically induced mechanical motions, such as shock, acoustic and ultrasound waves, and cavitation bubbles. Special emphasis is given to the recent investigations of linear momentum transformation during the laser–material interaction and to the on-line monitoring of laser material processing.

1 Introduction

"Optodynamics" [1] is defined as an interdisciplinary research field, which deals with the dynamic (mechanical) aspects of the interaction between light and matter. In accordance with this definition, a wide spectrum of phenomena can be associated with optodynamics: high-intensity photo-acoustics, which includes light-induced mechanical motion [2], laser-induced shock waves and cavitation bubbles in fluids [3, 4], laser propulsion [5, 6], a wide variety of laser material processes [7, 8], and laser-assisted medical applications, such as intraocular microsurgery [3, 9] and laser lithotripsy [10]. Here, it should be noted that optodynamics should not be confused with photodynamic therapy [11], which means photo-activation without any macroscopic material motion.

J. Možina (✉) · J. Diaci
Faculty of Mechanical Engineering, University of Ljubljana,
Aškerčeva 6, 1000 Ljubljana, Slovenia
e-mail: janez.mozina@fs.uni-lj.si

The optical-to-mechanical energy conversion efficiency increases from the thermoelastic regime to high-power pulsed laser processes [12]. The single pulse dynamics on the micro and millimeter scale can be followed by macroscopic effects. In the case of the solid state materials, these effects include bending, surface spallation, and breaking and expansion of ablated material [13, 14]. On the other hand, the optical energy in fluids is converted into the mechanical energy of shock waves and cavitation bubbles [3, 4].

Figure 1 shows a schematic of optodynamic phenomena that occur during pulsed laser–material interaction. Material irradiated by short laser pulses becomes rapidly overheated locally. Its temperature may exceed vaporization temperature, the mixture of vapor and the surrounding gas may become ionized forming a plasma cloud above the irradiated surface. This local thermal inequilibrium relaxes through the emission of light, heat conduction, and various forms of macroscopic material motion, e.g., mechanical waves that propagate through the workpiece and the surrounding media.

In view of laser material processing, a laser beam is not only considered as a tool but also as a generator of information about the material's transformation. The information is retained and conveyed by different kinds of optically induced mechanical waves. Several generation/detection schemes have been developed to extract this information especially in the field of laser ultrasonics (e.g., for non-destructive material evaluation) [15, 16]. In a wider aspect, these techniques can be used for optodynamic monitoring and the characterization of laser cutting, drilling, welding, and other pulsed-laser material processes [7, 17–20]. Blast, acoustic, and shock waves, which propagate in the fluid (gasses or liquids) surrounding the workpiece, have been studied using microphone detection [21] as well as various set-ups of the laser beam deflection probe [12, 22–24].

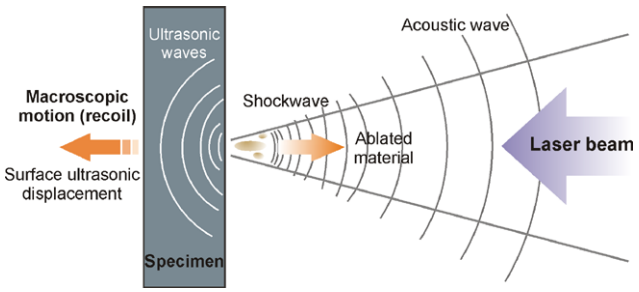

Fig. 1 Optodynamic phenomena during laser–material interaction

These techniques provide time resolved information at certain points in space. Various fast imaging techniques [3, 25, 26] have been used on the other hand to acquire spatially resolved information at certain points in time. Ultrasonic waves propagating through the workpiece have been studied using piezoelectric transducers [27] and laser interferometers [28].

This contribution presents recent results in the area of laser–material interaction with a special emphasis on the optodynamic aspects of this interaction, which includes the links between the laser material removal and the resulting material motion. Special attention is given to the linear momentum transformation, which has been studied with a homodyne quadrature laser interferometer [29, 30] and to the on-line monitoring of laser material processes, such as real-time monitoring of laser drilling.

2 One-dimensional linear model

Here, we will present a one-dimensional mathematical model of thermoelastic-wave generation due to laser-light absorption in solids [31, 32]. The model consists of a semi-infinite, transparent backing material through which the incident light propagates ($x < 0$), and a light-absorbing semi-infinite sample ($x > 0$). In addition, a realistic picture of the interaction between the light beam and the sample surface is taken into account by the consideration of the heat diffusion, the exact thermal and mechanical conditions, and the arbitrary time dependency of incident light-beam intensity. One of the possible experimentally compatible configurations is a uniformly illuminated layer. Since a detailed description of this model can be found in [32], we will present here only the final results.

In the approximation of this model, the sample surface is at $x = 0$. It is assumed that the semi-infinite backing material through which the light propagates ($x < 0$) is transparent, and its thermal conductivity is zero. If the sample surface is illuminated uniformly, the problem is one dimensional. So, we can evaluate the temperature field $T = T(x, t)$ and the elastic-displacement field $u = u(x, t)$ by a system of thermoelastic equations:

$$\begin{aligned} &\lambda T_{xx} = \rho c_v (T_t + \gamma T_0 u_{xt}) - w(x,t), \\ &c^2 u_{xx} = u_{tt} + \gamma c_v T_x \quad \text{for } x > 0, \\ &T = T_0, \qquad c_1^2 u_{xx} = u_{tt} \quad \text{for } x < 0, \end{aligned} \tag{1}$$

where γ is Grünesien's constant [33]. For most metals, the values are ≈ 1. In (1), λ stands for the thermal conductivity, ρ is the mass density, c_v is the thermal specific heat capacity, and c and c_1 are the speed of sound in the semiinfinite sample $x > 0$, and in the backing material $x < 0$, respectively.

Assuming that the absorbed light with intensity $I(t)$ is converted into heat fast enough, the volume power density of the laser-heating source $w(x, t)$ in (1) can be defined as

$$w(x,t) = a\mu \exp(-\mu x) I(t), \tag{2}$$

where a and μ are the surface absorptivity and the attenuation coefficient, respectively. The dimensionless variables for time, length, and attenuation:

$$\tau = \frac{t}{t_k}, \qquad \xi = \frac{x}{ct_k}, \qquad p = \mu c t_k \tag{3}$$

can be introduced by the characteristic thermoelastic time t_k, defined by the parameters of the solids [31, 32]:

$$t_k = \frac{\lambda}{c_v E}, \tag{4}$$

where E stands for Young's modulus. For most metals, t_k is in the order of magnitude of 10^{-11} s. This corresponds to the time needed for the conversion of the optical energy into the energy of the optodynamic wave.

Solving (1) after the consideration of appropriate initially and boundary conditions [32] give the total displacement of the front surface:

$$u_0 = -\frac{a\gamma q}{(1+K)E}. \tag{5}$$

Here, q stands for the density of the absorbed energy and $K = (\rho_1 c_1)/(\rho c)$ is the ratio of the mechanical impedances of the solid and the backing material.

Equation (5) shows that the final displacement does not depend on the pulse duration—it depends only on the density of the absorbed laser-energy.

Figure 2 shows the displacement of the surface at position $x = ct$ as a function of the reduced time $t_R = t - x/c$. The presented analytical solution was derived for a 1 mm-thick aluminum plate irradiated with a laser pulse having a fluency of 150 J/m^2 and a duration of 20 ns.

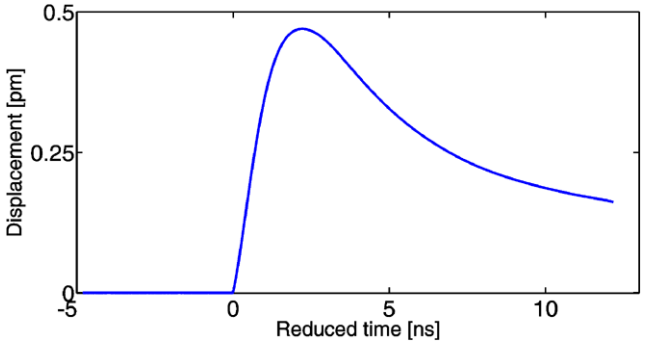

Fig. 2 The displacement of the surface at position $x = ct$ as a function of the reduced time

3 Optodynamic energy conversion

Shock waves generated during the interaction of short high-power laser pulses with a solid material, convey useful information that can be employed to monitor the process. A quantitative parameter that can be used for this purpose is, e.g., the energy E_h, contained within a shock wave. E_h can be determined from a spherical shock wave using the Taylor–Sedov point explosion theoretical model. The solutions of the model are expressed in terms of dimensionless space $\xi = r/r_c$ and time $\tau = t/t_c$ coordinates with characteristic scaling parameters:

$$r_c = (\alpha E/p_0)^{1/3} \quad \text{and} \quad t_c = r_c/c_0 \tag{6}$$

that depend on blast energy E, pressure p_0 and sonic velocity c_0 of the undisturbed gas and $\alpha = 1.175$ for air.

We employ the theoretical shock trajectory $\tau_s = f_1(\xi_s)$ adopted from a published numerical solution [34] to determine the blast energy from the measured data. A point of the shock trajectory is obtained by measuring the shock transit time t_s at a certain distance r_s from the ablated surface.

We have developed two methods that allow the experimental characterization of the shock trajectory and the determination of E_h for single and nonreproducible optodynamic events. The multiple-pass laser beam deflection (LBD) arrangement [35] gives us the possibility of acquiring temporally resolved information (signal waveforms) on single and nonreproducible events in several points of space. For each shock wave, we determine its wavefront transit times at several points in space from a single oscilloscope trace and fit the data to the theoretical shock trajectory in order to determine the blast energy released in the shock wave.

Rather than actually measuring the distance r_s in this case, we measure the acoustic wave transit time t_a in the same configuration. We produce the acoustic wave by decreasing the incident laser energy below the ablation threshold. From the shock and acoustic waveforms, we obtain multiple trajectory points (t_{si}, t_{ai}) for each shock wave. By fitting the measured points (t_{si}, t_{ai}) to the theoretical trajectory using a nonlinear fitting procedure, we determine the characteristic time t_c of the ablation event:

$$t_{si}/t_c = f(t_{ai}/t_c). \tag{7}$$

The other method is based on a novel double-exposure shadowgraphy set-up which allows the visualization of an expanding shock wave in two (or more) time instances on a single image [26]. The shock wave is illuminated by pulsed green laser light coupled into two (or more) optical fibers of different lengths to establish two illumination flashes separated by a fixed time delay. An image of the shock wave region, acquired using a digital still camera, exhibits two well separated shock wavefronts. The arrangement allows the acquisition of spatially resolved information on single and nonreproducible shock events in two (or more) time instances.

From the image, we extract two (or more) trajectory points (t_{si}, r_{si}) for each shock wave. By fitting the measured points (t_{si}, r_{si}) to the theoretical trajectory using a nonlinear fitting procedure we determine the characteristic time t_c of the ablation event:

$$t_{si}/t_c = f(r_{si}/c_0 t_c). \tag{8}$$

This multiple-point procedure improves the accuracy and reliability of the blast energy measurement. We assume that the energy E_h contained in a hemispherical wave is a half of the blast energy E that would produce the same mechanical effect in the spherical case and then determine E_h from [12]:

$$E_h = p_0(c_0 t_c)^3/2\alpha. \tag{9}$$

As an illustration of the result, we show in Fig. 3 the ratio E_h/E_l which we call the energy conversion efficiency, as a function of the incident laser energy E_l. The efficiency increases with the incident energy: quite rapidly at low E_l and only gradually at high E_l. In the low E_l range we also find that the pulse-to-pulse variations of the blast energy are much larger than the variations of incident energy, while in the high E_l range they are comparable.

Although the two methods provide essentially the same result, the practice shows that they are in fact complementary. The LBDP method is more suitable for weak shocks that exhibit a poor contrast relative to the background in the shadowgraphy images. The shadowgraphy method is more suitable for strong shocks and allows the assessment of the sphericity of the shock wave, and thus the verification of the basic assumption underlying the methods.

4 Linear momentum transformation

The *transfer* of the linear momentum to the specimen during the laser pulse–material interaction has been thoroughly

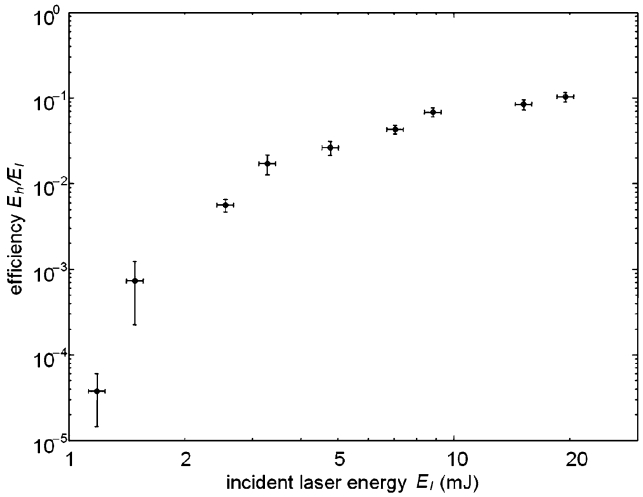

Fig. 3 Energy conversion efficiency versus incident laser energy during laser ablation of a steel sample

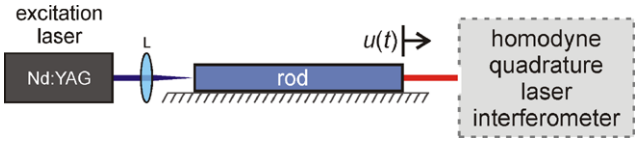

Fig. 4 Schematic diagram of the experimental set-up. The front end of the rod is illuminated by a single Nd:YAG 10-ns pulse with the energy of 300 mJ. The axial displacement of the rod's rear end is measured with the homodyne quadrature laser interferometer (HQLI)

studied using various ballistic measurements [36–40] and analytical/numerical calculations [41–43], while the linear-momentum *flow* [44–46] at the pulsed-ablation of the material is a novelty in the assessments of laser material processing.

Apart from the transfer and flow of laser pulse *energy,* the *linear momentum* is often a set-aside aspect of optodynamics even though it deserves a great deal of attention, for example, in the studies of laser-ablation-assisted localized drug delivery [47] and ablative laser-driven propulsion [5, 6].

We investigated the flow of linear momentum both experimentally and theoretically for the case of elastic steel rods [44, 45]. For this purpose, we developed a contactless homodyne quadrature laser interferometer (HQLI) featuring a wide dynamic range and nanometre resolution [46]. We explained how a rod acquires linear momentum [44, 45] and analyzed the effects of dispersion [28] on its transfer from the initial mechanical wave to the whole sample. The key linear-momentum sink mechanisms are friction and its transmission to the ambient air [30].

For example, the standard figure of merit for the effectiveness of the light-matter interaction in the ablative laser propulsion is the laser momentum coupling coefficient $C_\mathrm{m} = p/E$, defined as the ratio of a laser-formed linear momentum p obtained by the target and the laser pulse energy E. This physical quantity depends strongly on the pulse duration, target material properties, ambient air pressure, and laser-pulse intensity. Its unknown behavior can be conveniently inferred by monitoring the flow of linear momentum.

When the front side of a steel rod is struck by a short laser pulse that surpasses the ablation threshold (see Fig. 4), the light-matter interaction yields many optodynamic processes, including: mass removal, plasma formation, the generation of ultrasonic waves in the sample and detonation/pressure waves in the surrounding air. The conservation of the linear momentum demands that the rod must obtain an opposite equal momentum compared to all of the material from which the rod has been pushed away (see Fig. 4). This momentum is not acquired by the whole rod at once. Initially, it is localized inside the laser generated ultrasonic wave which travels along the rod. During the propagation of the wave and its many reflections at the specimen's boundaries, the momentum of the wave is gradually transferred to the bulk medium—the rod as a whole. Finally, all of the momentum encompassed in the initial ultrasonic wave is converted to a uniform movement of the rod. If at the beginning only the particles inside the ultrasonic wave are those which move, and thus carry the momentum as they propagate as a wave motion, in the end all parts of the rod achieve the same velocity after the ultrasonic wave completely dies away.

The nature of the interaction between the laser pulse and the material is visible in Fig. 5. Here, the motion immediately after the laser pulse is restricted to the mechanical wave. This wave is much shorter compared to the length of the rod L. After the time-of-flight $t_L = L/c_0 = 23.5$ µs—the time needed for the wave to reach the other end of the rod—the reflection of the mechanical wave causes a displacement of the rear end of the rod. c_0 is the elementary thin-rod velocity. However, after the reflection, the end cross-section does not return to the initial position. This happens on every return n of the wave to the rear end at times $t = (1 + 2n)t_L$, leading to the discrete steps superimposed on a uniform motion. Figure 5a reveals that the mechanical wave concealed in the elastic body is responsible for its motion. The motion takes place only within the mechanical wave; the other parts of the rod are at rest. This is very clearly seen in the first few steps (a few hundred µs) in Fig. 5b when the influence of the friction and dispersion is sufficiently small. Later on, the dispersion widens the initially short wave until the wave's length becomes comparable to the length of the rod. This is one of the mechanisms of the linear momentum transfer from the mechanical wave to the whole body.

The laser-induced mechanical wave is a short compression/rarefaction; therefore, it is comprised of high-frequency components. The Fourier components of different frequencies travel with different phase velocities according to the

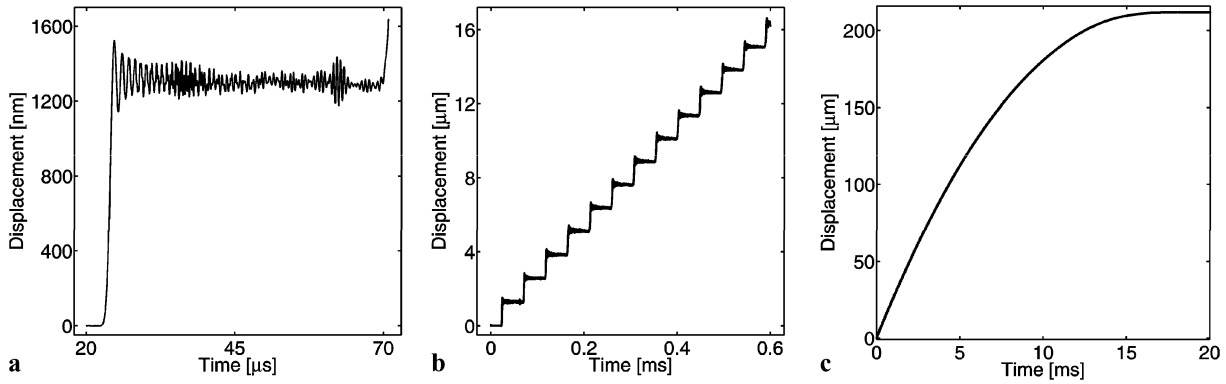

Fig. 5 The motion of a laser-ablated rod that moves in a step-like fashion until it stops due to friction. The axial displacement was measured in a single shot with the HQLI at the rear end of the 120 mm-long steel rod as a function of time. **a** Magnification of the first step. The high-frequency oscillations caused by the wave's geometrical dispersion are clearly seen. **b** Magnification of the displacement shows that the rear end moves in abrupt discrete steps that are superimposed on a uniform motion. **c** The entire motion of the rod's rear end after laser ablation

dispersion relations. The effects of the geometric dispersion add a tail of alternating particle velocities to the wave's front. At the first arrival to the rear end, the wave's front is 1 µs wide and displaces the rod's rear end by the height (1.3 µm) of a step (Fig. 5a). The vibrating motion of the rear end in the time interval between 23.5 and 35 µs is caused by the lateral inertia. The proceeding subtle displacements around the general step height before the arrival of the next wave correspond to the rich structure of the Pochhammer–Chree (PC) dispersion relations for the axisymmetric, longitudinal, time-harmonic waves in an infinite rod. The arrival of the second PC mode is visible from 29 µs on as a few MHz oscillations superimposed on the dominant carrier frequency.

5 Monitoring of laser drilling

Laser micro-drilling using short laser pulses in the nanosecond or sub-nanosecond range is a typical optodynamic phenomenon, where the interaction between the laser light and the material induces a mechanical dynamic process. The process can be described by two phenomena. Firstly, due to the focused laser pulse with high intensity that interacts with the material surface, plasma and hot gasses appear resulting in a micro-explosion. Secondly, the formation of the micro-explosion represents a source of a pressure front or shock wave propagating into the sample and the surrounding atmosphere. By detecting either or both of these dynamic processes one can study, monitor or control the process. Firstly, the shock wave propagating within the sample can be measured using, for example, piezoelectric elements or by noncontact optical methods based on different types of interferometric techniques [48, 49]. Secondly, the plasma and the shock wave propagating into the surrounding atmosphere can be measured using one of several optical methods, for example, a beam-deflection probe (BDP) [12, 50–55].

Optodynamic detection methods have been successfully applied to develop a reliable method for drilling specified micro-holes into glass ampoules and vials [54]. Test ampoules with holes are used in pharmaceutical production lines for the adjustment of high-voltage leak-detection devices. Figure 6 shows a set-up that has been used in validation of the method. The processing UV beam, emitted from a frequency multiplied Nd:YAG laser, is focused on the front surface of the 5 mm thick glass sample. The parameters of the laser processing beam are as follows: wavelength 266 nm, pulse duration 6 ns, pulse energy 1 mJ, repetition rate 10 Hz, and the NA of the lens was 0.05.

The drilled hole is simultaneously monitored by a microscope camera and an interferometer which detects the ultrasonic transients that are generated during the drilling pulses and propagate through the glass. In order to suppress the vibration from the environment, the interferometer has a compensated reference arm. The length of this arm is controlled by a piezoelectric element driven by a PID closed loop [56]. To get adequate reflection of the probe beam from the interferometer measuring arm, the rear surface of the sample has been polished and gold plated. The hole depth is determined from the time of flight of the ultrasonic wave that travels from the bottom of the hole to the rear surface of the sample where it is detected by the interferometer. The microscope camera is used to verify the data of the hole depth obtained from the interferometric measurement.

Figure 7 shows the evolution of the hole depth recorded by the two methods during a sequence of consecutive laser pulses. It is evident that the hole depth obtained from the time-of-flight measurement agrees very well with the one obtained from the microscope observation. The interferometric method can therefore be used for on-line monitoring for the laser micro-drilling process in cases where the hole

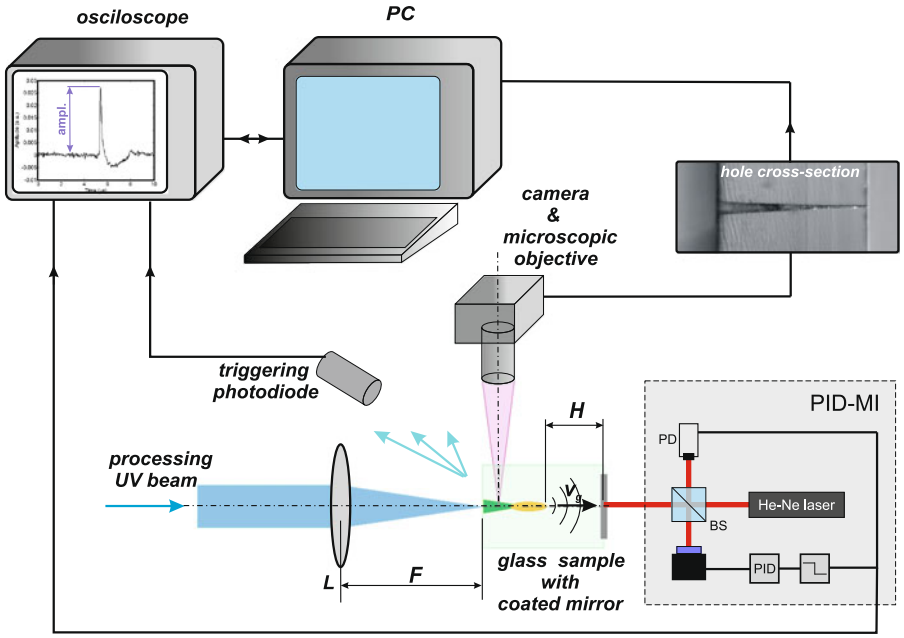

Fig. 6 Setup for monitoring the hole depth during laser micro-drilling

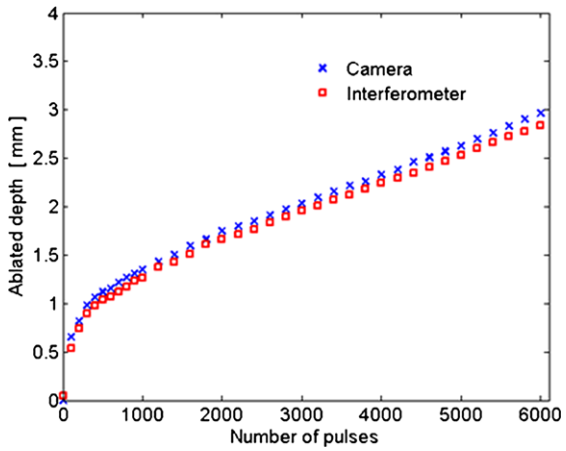

Fig. 7 The hole depth during glass micro-drilling as obtained from the interferometric measurements. The measurements from the microscope camera are included in the graph for comparison

cannot be imaged through the wall, e.g., when drilling complex surfaces (ampoules,) or nontransparent materials.

6 Conclusion

The paper reports the results of recent investigations in the field of optodynamics focusing on linear momentum transformation during the laser–material interaction and on-line monitoring of laser material processing. The results demonstrate that research methodologies developed within the field of optodynamics can be successfully applied to study a wide spectrum of phenomena and laser applications.

References

1. J. Možina, R. Hrovatin, Prog. Nat. Sci. **6**, S709 (1996)
2. A.C. Tam, Rev. Mod. Phys. **58**, 381 (1986)
3. E.A. Brujan, A. Vogel, J. Fluid Mech. **558**, 281 (2006)
4. P. Gregorčič, R. Petkovšek, J. Možina, G. Močnik, Appl. Phys. A, Mater. Sci. Process. **93**, 901 (2008)
5. A. Kantrowitz, Astronaut. Aeronaut. **10**, 74 (1972)
6. K. Anju, K. Sawada, A. Sasoh, K. Mori, E. Zaretsky, J. Propuls. Power **24**, 322 (2008)
7. R. Hrovatin, J. Možina, Appl. Surf. Sci. **86**, 213 (1995)
8. L. Grad, J. Možina, Lasers Eng. **4**, 255 (1995)
9. A. Vogel, P. Schweiger, A. Frieser, M.N. Asiyo, R. Birngruber, IEEE J. Sel. Top. Quantum Electron. **26**, 2240 (1990)
10. A. Vogel, Phys. Med. Biol. **42**, 895 (1997)
11. E. Unsold, D. Jocham, Chirurg **59**, 76 (1988)
12. J. Diaci, J. Možina, Ultrasonics **34**, 523 (1996)
13. R.M. Gilgenbach, P.L.G. Ventzek, Appl. Phys. Lett. **58**, 1597 (1991)
14. C.W. White, P.P. Pronko, S.R. Wilson, B.R. Appleton, J. Narayan, R.T. Young, J. Appl. Phys. **50**, 3261 (1979)
15. S.N. Hopko, I.C. Ume, J. Nondestruct. Eval. **18**, 91 (1999)
16. R. Hrovatin, R. Petkovšek, J. Diaci, J. Možina, Ultrasonics **44**, e1199 (2006)
17. R.E. Wagner, J. Appl. Phys. **45**, 4631 (1974)
18. V. Kovalenko, R. Zhuk, J. Mater. Process. Technol. **149**, 553 (2004)
19. M. Jezeršek, V. Gruden, J. Možina, Opt. Express **12**, 4905 (2004)
20. R. Petkovšek, J. Možina, J. Appl. Phys. **102**, 044905 (2007)
21. A. Gorkič, D. Kovačič, J. Diaci, Int. J. Adv. Manuf. Technol. **42**, 138 (2009)
22. J. Diaci, Rev. Sci. Instrum. **63**, 5306 (1992)
23. R. Petkovšek, P. Gregorčič, J. Možina, Meas. Sci. Technol. **18**, 2972 (2007)
24. D. Horvat, R. Petkovšek, J. Možina, Meas. Sci. Technol. **21**, 035301 (2010)
25. R. Petkovšek, P. Gregorčič, J. Appl. Phys. **102**, 044909 (2007)
26. T. Perhavec, J. Diaci, Stroj. Vest., J. Mech. Eng. Sci. **56**, 477 (2010)
27. S. Strgar, J. Možina, Ultrasonics **40**, 791 (2002)

28. T. Požar, R. Petkovšek, J. Možina, Appl. Phys. Lett. **92**, 234101 (2008)
29. T. Požar, P. Gregorčič, J. Možina, Opt. Express **17**, 22906 (2009)
30. T. Požar, J. Možina, Stroj. Vest., J. Mech. Eng. Sci. **55**, 575 (2009)
31. J. Možina, Ph.D. thesis, Faculty of Mechanical Engineering, Ljubljana 1980 (in Slovene)
32. J. Možina, M. Dovč, Mod. Phys. Lett. B **8**, 1791 (1994)
33. B.H. Flowers, E. Mendoza, *Properties of Matter* (Wiley, London, 1970)
34. D.E. Okhotsimskii, Z.P. Vlasova, J. Vychisl. Mat. Mat. Fiz. **2**, 107 (1962) (in Russian)
35. J. Diaci, J. Možina, Rev. Sci. Instrum. **66**, 4644 (1995)
36. D.W. Gregg, S.J. Thomas, J. Appl. Phys. **37**, 2787 (1966)
37. D.J. Lee, S.H. Jeong, Appl. Phys. A, Mater. Sci. Process. **79**, 1341 (2004)
38. Z.Y. Zheng, J. Zhang, X. Lu, Z.Q. Hao, X.H. Yuan, Z.H. Wang, Z.Y. Wei, Appl. Phys. A, Mater. Sci. Process. **83**, 329 (2006)
39. C. Phipps, J. Luke, D. Funk, D. Moore, J. Glownia, T. Lippert, Appl. Surf. Sci. **252**, 4838 (2006)
40. K. Watanabe, K. Mori, A. Sasoh, J. Propuls. Power **22**, 1149 (2006)
41. A.N. Pirri, R. Schlier, D. Northam, Appl. Phys. Lett. **21**, 79 (1972)
42. V. Semak, A. Matsunawa, J. Phys. D, Appl. Phys. **30**, 2541 (1997)
43. S.B. Wen, X.L. Mao, R. Greif, R.E. Russo, J. Appl. Phys. **101**, 023114 (2007)
44. T. Požar, J. Možina, Appl. Phys. A, Mater. Sci. Process. **91**, 315 (2008)
45. T. Požar, R. Petkovšek, J. Možina, Appl. Phys. A, Mater. Sci. Process. **92**, 891 (2008)
46. P. Gregorčič, T. Požar, J. Možina, Opt. Express **17**, 16322 (2009)
47. V. Menezes, K. Takayama, T. Ohki, J. Gopalan, Appl. Phys. Lett. **87**, 163504 (2005)
48. Q. Shan, A.S. Bradford, R.J. Dewhurst, Meas. Sci. Technol. **9**, 24 (1998)
49. B.P. Payne, V. Venugopalan, B.B. Mikic, N.S. Nishioka, J. Biomed. Opt. **8**, 264 (2003)
50. M. Villagran-Muniz, H. Sobral, R. Navarro-Gonzalez, Meas. Sci. Technol. **14**, 614 (2003)
51. S.H. Jeong, R. Greif, R.E. Russo, J. Phys. D, Appl. Phys. **32**, 2578 (1999)
52. S.R. Franklin, P. Chauhan, A. Mitra, R.K. Thareja, J. Appl. Phys. **97**, 094919 (2005)
53. S. Strgar, J. Možina, Appl. Phys. A **74**, 321 (2002)
54. R. Petkovšek, A. Babnik, J. Diaci, Meas. Sci. Technol. **17**, 2828 (2006)
55. R. Petkovšek, J. Možina, J. Appl. Phys. **102**, 44905 (2007)
56. R. Petkovšek, I. Panjan, A. Babnik, J. Možina, Ultrasonics **44**, 1191 (2006)